Quantum wires in magnetic field: a comparative study of the Hartree–Fock and the spin density functional approaches



2008 J. Phys.: Condens. Matter 20 335233

(http://iopscience.iop.org/0953-8984/20/33/335233)

J. Phys.: Condens. Matter **20** (2008) 335233 (5pp) doi:10.1088/0953-8984/20/33/335233

# Quantum wires in magnetic field: a comparative study of the Hartree–Fock and the spin density functional approaches

**S Ihnatsenka and I V Zozoulenko**

Solid State Electronics, Department of Science and Technology (ITN), Linköping University, SE-60174 Norrköping, Sweden

Received 24 April 2008, in final form 19 June 2008
Published 31 July 2008
Online at stacks.iop.org/JPhysCM/20/335233

**Abstract**

We present a detailed comparison of the self-consistent calculations based on the Hartree–Fock and the spin density functional theory for a split-gate quantum wire in the IQH regime. We demonstrate that both approaches provide qualitatively (and, in most cases, quantitatively) similar results for the spin-resolved electron density, spin polarization, spatial spin separation at the edges and the effective $g$ factor. Both approaches produce the same values of the magnetic fields corresponding to the successive subband depopulation and qualitatively similar evolution of the magnetosubbands. Quantitatively, however, the HF and the DFT subbands are different (even though the corresponding total electron densities are practically the same). In contrast to the HF approach, the DFT calculations predict much larger spatial spin separation near the wire edge for the low magnetic fields (when the compressible strips for spinless electrons are not formed yet). In the opposite limit of the large fields, the Hartree–Fock and the DFT approaches give very similar values for the spatial spin separation.

(Some figures in this article are in colour only in the electronic version)

## 1. Introduction

A detailed knowledge of energetics, spin splitting, magnetosubband and edge state structure in quantum wires is necessary for the understanding and interpretation of a variety of magnetotransport phenomena in the integer quantum Hall (IQH) regime. A powerful tool to study electron–electron interaction and spin effects in quantum wires is the mean-field approach such as the Hartree–Fock (HF) and the spin density functional theory (DFT) [1]. A number of studies based on these approaches addressing various aspects of interacting electrons in the IQH regime in quantum wires have been reported recently [2–17]. However, in some cases different studies produce different results and findings reported in some studies are not recovered in others. It is not clear whether this is due to using different approaches treating the exchange and correlation effects in different ways (i.e. HF vs spin DFT), or if this difference is related to various approximations of different models (such as, for example, neglecting a global electrostatics, simplified models for screening, non-self-consistent calculations, fixed filling factors, etc).

The main aim of this paper is to present a detailed comparison of the self-consistent calculations based on the HF method and the spin DFT approximation for a split-gate quantum wire in the IQH regime. This includes a comparison of the magnetosubband structure, electron densities, spin polarization and spatial spin separation as well as calculation of the effective $g$ factor. We stress that in our calculations we do not use any simplified assumptions concerning screening, so the global electrostatics of the system at hand are treated exactly. Note that comparative studies of different approaches are common in the treatment of electronic properties of quantum dots as they provide an important insight into the validity of applied methods and approximations used [18]. At the same time, we are not aware of corresponding studies for the quantum wires in the IQH regime.

## 2. Basics

We consider an infinitely long split-gate GaAs/AlGaAs quantum wire in a perpendicular magnetic field $B$ where electrons are situated at a distance $b$ below the surface. The HF equation for a single-particle wavefunction of spin $\sigma$, $\Phi^{\sigma}_{\beta}(\mathbf{r})$ is [1]

 

$$\left[H_0(\mathbf{r}) + V_{\rm conf}(y) + V_H(y) + V_Z\right]\Phi^\sigma_\beta(\mathbf{r}) + \int V_{\rm Fock}(\mathbf{r},\mathbf{r}')\Phi_\beta(\mathbf{r}')\,{\rm d}\mathbf{r}' = E_\beta\Phi^\sigma_\beta(\mathbf{r}), \quad (1)$$

where $\mathbf{r} = (x, y)$, $H_0(\mathbf{r}) = -\frac{\hbar^2}{2m^*}(\frac{\partial}{\partial x} - \frac{eiBy}{\hbar})^2 + \frac{\partial^2}{\partial y^2}$ is the kinetic energy in the Landau gauge, with $m^* = 0.067m_{\rm e}$ being the GaAs effective mass; $\sigma = \pm\frac{1}{2}$ describes spin-up and spin-down states, $\uparrow$, $\downarrow$. In the split-gate geometry the bare confining potential $V_{\rm conf}(y)$ due to the gates, donor layers and the Schottky barrier is well approximated by the parabolic confinement, $V_{\rm conf}(y) = V_0 + \frac{m^*}{2}(\omega_0 y)^2$, where $V_0$ defines the bottom of the potential (we set the Fermi energy $E_{\rm F} = 0$) [14]. The Zeeman energy is $V_Z = g\mu_b B\sigma$ where $\mu_{\rm B} = e\hbar/2m_{\rm e}$ is the Bohr magneton and the bulk $g$ factor of GaAs is $g = -0.44$. The Hartree potential due to the electron density $n(y) = \sum_\sigma n^\sigma(y)$ is [14] $V_H(y) = -\frac{e^2}{4\pi\varepsilon_0\varepsilon_r}\int {\rm d}y' n(y') \ln\frac{(y-y')^2}{(y-y')^2+4b^2}$. (This term includes mirror charges that account for the fact that the GaAs surface is at the same potential everywhere due to the surface states that pin the chemical potential to the energy in the middle of the gap [19].) The nonlocal Fock operator is $V_{\rm Fock}(\mathbf{r},\mathbf{r}') = -\frac{e^2}{4\pi\varepsilon\varepsilon_0|\mathbf{r}-\mathbf{r}'|}\sum_\beta f^{\rm FD}_{E_\beta}\Phi^\sigma_\beta(\mathbf{r})\Phi^{\sigma *}_\beta(\mathbf{r}')$, where the summation is performed over all states $\beta$ and $f^{\rm FD}_{E_\beta}$ is the Fermi–Dirac distribution function.

We assume the Bloch form of the wavefunction:

$$\Phi^\sigma_{n,k}(x, y) = {\rm e}^{{\rm i}kx}\varphi^\sigma_{n,k}(y) \quad (2)$$

where $k$ is the wavevector and $\varphi^\sigma_{n,k}(y)$ describes the $n$th transverse subband for the spin $\sigma$. Substituting the Bloch function (2) into the HF equation (1) and integrating over the longitudinal coordinate $x$ we arrive at the eigenequations for $\varphi^\sigma_{n,k}(y)$ [9]:

$$\left[-\frac{\hbar^2}{2m^*}\frac{{\rm d}^2}{{\rm d}y^2} + \frac{m^*\omega_{\rm c}^2}{2}\left(y + \frac{\hbar k}{eB}\right)^2 + V_{\rm conf}(y) + V_H(y) + V_Z\right]\varphi^\sigma_{n,k}(y) + \int V^k_{\rm Fock}(y, y')\varphi^\sigma_{n,k}(y')\,{\rm d}y' = E^\sigma_{n,k}\varphi^\sigma_{n,k}(y), \quad (3)$$

where $\omega_{\rm c}$ is the cyclotron frequency and

$$V^k_{\rm Fock}(y, y') = -\frac{e^2}{2\pi\varepsilon_0\varepsilon_r}\sum_{n'k'} f^{\rm FD}_{E^\sigma_{n,k}}\varphi^\sigma_{n'k'}(y)\varphi^{\sigma *}_{n'k'}(y') \times K_0\left(|k - k'||y - y'|\right), \quad (4)$$

with $K_0$ being the modified Bessel function. Discretizing equation (3) we reduce the system of the integro-differential equations to the system of linear equations, which we solve numerically by standard methods in an iterative way until the self-consistent solution is achieved. Knowledge of the wavevectors $k^\sigma_n$ for different states $\{n, \sigma\}$ allows us to recover the subband structure [14], i.e. to calculate an average position $y^\sigma_n$ of the wavefunctions for different modes $n$, $y^\sigma_n = \hbar k^\sigma_n/eB$ [19].

Within the framework of the spin density functional theory, the Kohn–Sham equations for the single-particle wavefunction $\Phi^\sigma_\beta(\mathbf{r})$ are [1]

$$\left[H_0(\mathbf{r}) + V^\sigma(y)\right]\Phi^\sigma_\beta(\mathbf{r}) = E_\beta\Phi^\sigma_\beta(\mathbf{r}), \quad (5)$$

$$V^\sigma(y) = V_{\rm conf}(y) + V_H(y) + V_Z + V^{\sigma,\zeta}_{\rm xc}(y), \quad (6)$$

where the first three terms in the effective confinement potential $V^\sigma(y)$ are the same as in the HF equation (1) and the last term corresponds to the exchange and correlation potential in the local spin density approximation. It is given by the functional derivative $V^{\sigma,\zeta}_{\rm xc} = \frac{\delta}{\delta n^\sigma}\{n\epsilon^\zeta_{\rm xc}(n)\}$, where $\epsilon^\zeta_{\rm xc}(n)$ is the exchange and correlation energy functional and $\zeta(y) = \frac{n^\uparrow - n^\downarrow}{n^\uparrow + n^\downarrow}$ is the local spin polarization. All the results presented below correspond to the parameterization of $\epsilon^\zeta_{\rm xc}(n)$ given by Tanatar and Ceperley [20]. Assuming the Bloch form of the wavefunctions (2), equations (5) are solved self-consistently using the Green's function technique as described in detail in [14] (see also [15, 16]).

Note that we find the self-consistent solutions for the DFT and the HF approaches using completely unrelated numerical methods. As a validity check we control that these different methods give identical results when we set $V^k_{\rm Fock}$ and $V^{\sigma,\zeta}_{\rm xc}$ in, respectively, equations (3) and (6) to zero and thus reduce both approaches to the standard spinless Hartree approximation (the latter is shown to reproduce well [15, 22] the Chklovskii *et al* [21] electrostatic treatment).

## 3. Results and discussion

Figure 1 shows a spatially resolved difference in the electron density $n^\uparrow - n^\downarrow$ and the total spin polarization $P = \frac{n^\uparrow_{\rm 1D} - n^\downarrow_{\rm 1D}}{n^\uparrow_{\rm 1D} + n^\downarrow_{\rm 1D}}$ calculated using the HF and the spin DFT approaches for a representative quantum wire ($n^\sigma_{\rm 1D} = \int n^\sigma(y)\,{\rm d}y$). A detailed analysis of the spin polarization in a split-gate quantum wire based on the spin DFT approach was given in our previous work [14, 15]. For the sake of comparison with the HF approximation we summarize below the main findings. The spin polarization is maximal for magnetic fields close to depopulation of the even subbands, see figure 1(d). In this case the highest occupied (odd) subband forms a compressible strip in the middle of the wire and, therefore, the electron density is mostly spin-polarized in the center of the wire, see figure 2(d). (We define the width of the compressible strip within the window $|E - E_{\rm F}| \leqslant 2\pi kT$ [14–16, 22], which corresponds to the energy interval where the subbands are partially filled, $0 < f^{\rm FD} < 1$.) Minima of the spin polarization correspond, instead, to depopulation of the odd subbands. At polarization minima the spin-up and spin-down subbands are fully (and practically equally) occupied as their bottoms in the center of the wire are situated below (or just on the border) of the energy window $|E - E_{\rm F}| \leqslant 2\pi kT$, see figure 2(c). Spin polarization is absent in the center of the wire and increases towards the edges, because the spin-up and-down subbands intersect $E_{\rm F}$ at different distances from the wire center. For the case of spinless electrons compressible strips are formed near the wire boundaries for sufficiently high magnetic fields [15, 21, 22]. The exchange interaction, however, completely or partially suppress the compressible strips, leading to a spatial spin separation between the spin-up and spin-down states [15]. This spatial separation causes a strong spin polarization near the boundaries which is clearly seen in figure 1(b) for magnetic fields $B \gtrsim 2.75$ T. This

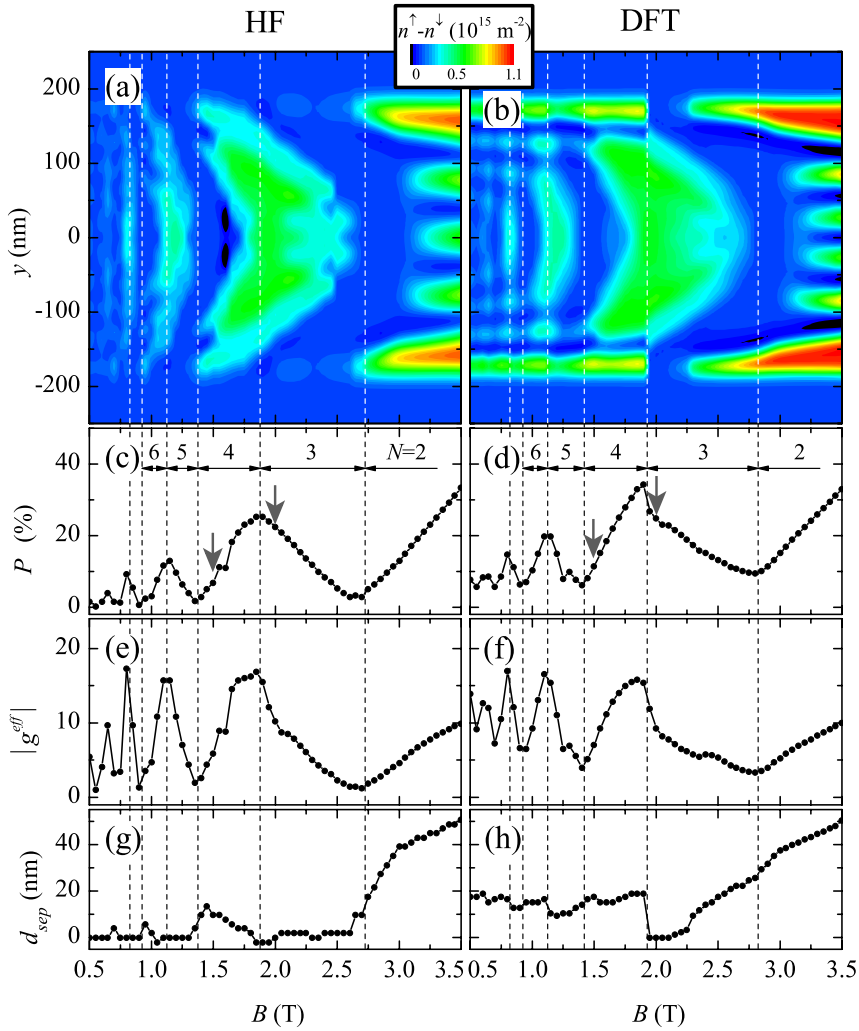


**Figure 1.** (a), (b) Spatially resolved spin polarization of the electron density $n^{\uparrow} - n^{\downarrow}$. (c), (d) the number of subbands and the total spin polarization $P = \frac{n_{1D}^{\uparrow} - n_{1D}^{\downarrow}}{n_{1D}^{\uparrow} + n_{1D}^{\downarrow}}$; arrows indicate the magnetic fields corresponding to the magnetosubband structure shown in figure 2. (e), (f) The effective $g$ factor. (g), (h) The spatial spin separation at the wire edge $d_{sep}$ (a definition of $d_{sep}$ is indicated at the right of figure 2(a)). The left and right panels correspond respectively to the HF and the spin DFT approximations. The bare confining potential $V_{conf}(y)$ is well approximated by parabolic confinement with $V_0 = -85$ meV, $\hbar\omega_c = 2$ meV, the distance to the surface $b = 60$ nm, temperature $T = 1$ K. With these parameters the linear electron density in the wire $n_{1D} = 5.5 \times 10^8$ m$^{-1}$ and the local (sheet) density in the wire center $n = 1.5 \times 10^{15}$ m$^{-2}$.

spin separation grows as the magnetic field increases because the width of the corresponding compressible strips for the spinless electrons increases, see figures 1(b) and (h). Note that the spin DFT approach also predicts an almost constant (independent of $B$) spatial spin polarization in the vicinity of wire boundaries (150 nm $\lesssim |y| \lesssim$ 200 nm) even for lower fields $B \lesssim 2.0$ T, when the compressible strips are not formed yet (cf. figures 1(a) and (b)). This low-field spin polarization near the wire boundaries is apparently absent in the HF approach.

Let us now compare the results of the spin DFT calculations with those based on the HF approach. It is remarkable that both approaches give practically the same values for the magnetic fields corresponding to the successive subband depopulation, cf. figures 1(c) and (d). Moreover, both approaches give practically the same *total* electron density distribution $n(y)$, see figures 2(a) and (b). However, the *spin-resolved* densities are not always the same. In contrast to the spin DFT approach, the HF calculation does not always exhibit a spatial spin polarization near the edges for the low fields (when the compressible strips for spinless electrons are not yet formed). This is the case for a quantum wire of figure 1 for $B \lesssim 2.75$ T. The spin separation near the wire edges $d_{sep}$ is caused by the exchange interaction and it is known to depend on the steepness of the confinement potential [3, 23]: as the external confining potential becomes smoother, the spin separation grows. Figure 3 shows that, while the spatial spin separation $d_{sep}^{DFT}$ and $d_{sep}^{HF}$ exhibit qualitatively the same behavior as a function of the potential steepness, the DFT approach predicts much larger spatial spin separation as compared to the HF method. Besides, the critical value of the potential steepness at which different spins become spatially separated is obviously lower in the HF approach. We stress that the difference between $d_{sep}^{DFT}$ and $d_{sep}^{HF}$ discussed

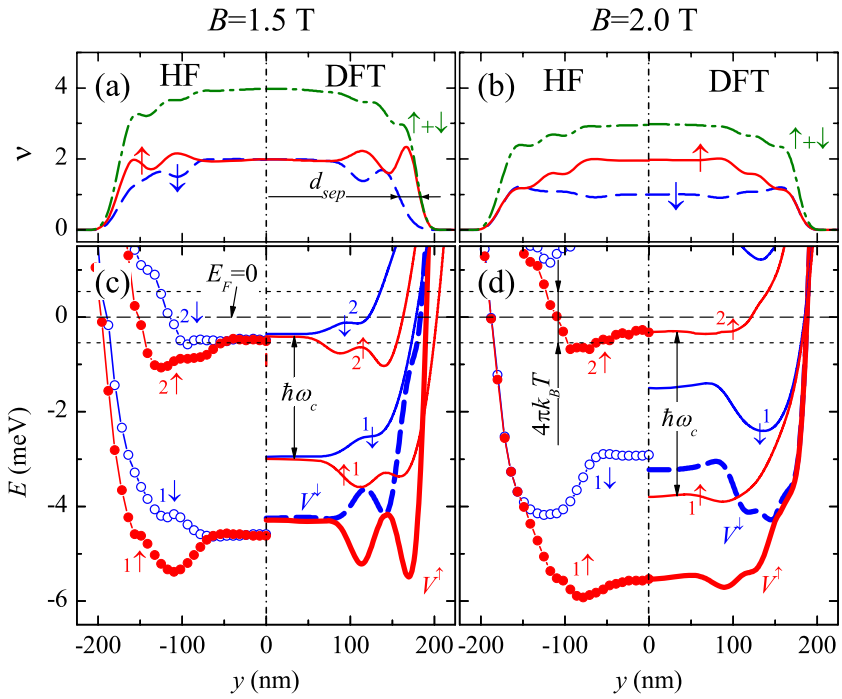


**Figure 2.** (a), (b) The local filling factors $\nu^{\uparrow}$, $\nu^{\downarrow}$ and $\nu = \nu^{\uparrow} + \nu^{\downarrow}$ ($\nu = nh/eB$) calculated within the HF and the spin DFT approaches for two representative magnetic fields (indicated by arrows in figures 1(c) and (d)). (c), (d) The magnetosubband structure for spin-up and spin-down electrons calculated within the HF and the spin DFT approaches. The thick solid lines indicate the DFT effective confinement potential $V^{\sigma}$, equation (6) (note that, because of the nonlocal character of the HF equations, it is not possible to define the effective confinement potential in the HF approach). $d_{\rm sep}$ defines a distance between up and down densities taken at a half-maximum of the density in the wire center.

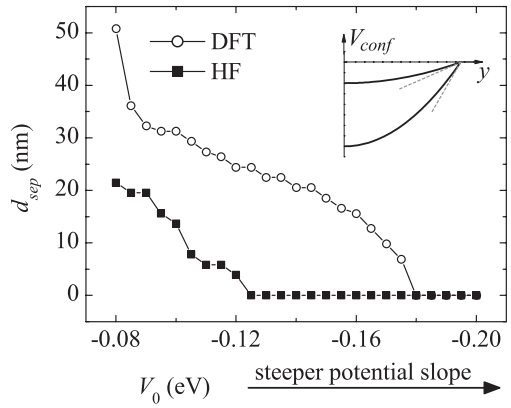


**Figure 3.** The spatial spin separation near the wire edge as a function of the confinement steepness calculated within the spin DFT and HF approaches in the regime of low fields ($B = 0.5$ T). The inset illustrates how the confinement steepness changes as the bottom of the parabolic confinement potential, $V_0$, varies ($\hbar\omega_0$ is adjusted to keep the wire width constant, $w = 500$ nm.)

above corresponds to the regime of the low fields, when the compressible strips for spinless electrons are not formed yet. For larger fields (corresponding to the formation of compressible strips for the spinless electrons), the Hartree–Fock and the DFT approaches give very similar values for the spin separation, cf. figures 1(g) and (h). In this case $d_{\rm sep}$ is approximately equal to the width of the compressible strips for spinless electrons (see [15] for a detailed discussion of the suppression of the compressible strips by the exchange interaction leading to the spatial spin polarization at the edges). Note that our study cannot distinguish which approach gives a correct result for $d_{\rm sep}$ for the low field. This question can be resolved by a comparison with the exact results obtained by, for example, quantum Monte Carlo methods. We speculate at this point that it is the DFT approach that overestimates the spatial spin separation at lower fields. This conclusion is based on transport measurements on lateral quantum dots, indicating that the spin-polarized injection and detection by means of the spatial separation of spins can be achieved only in the edge state regime for sufficiently high magnetic field [24].

Let us turn our attention to the subband structure. Figure 2 shows the subband structure for two representative magnetic fields corresponding to the minimum and maximum of the spin polarization in a quantum wire. Qualitatively, the HF and the DFT subbands exhibit very similar features and evolve in a similar way as the magnetic field is changed. This includes the subband depopulation, the formation of the compressible strip in the middle of the wire and the subband separation at the edges. Quantitatively, however, the HF and the DFT subbands are different (even though the corresponding densities are practically the same, see figures 2(b) and (d)). The most pronounced difference is that the consecutive subband separation for different spins in the DFT approach is equal to $\hbar\omega_{\rm c}$, whereas the HF subband separation exceeds this value. We attribute this difference to the nonlocal character of the exchange interaction in the HF approximation. Note that the HF subband separation tends to $\hbar\omega_{\rm c}$ as the density increases because the exchange interaction becomes less pronounced for higher densities in comparison to the kinetic energy.

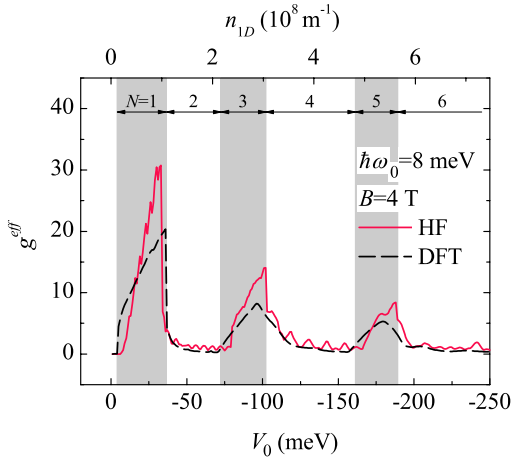


**Figure 4.** The effective $g$ factor as a function of $V_0$ (the potential bottom) calculated within the spin DFT and HF approaches. The magnetic field is $B = 4T$ and $\hbar\omega_0 = 8$ meV. $N$ indicates the number of occupied subbands.

Because the DFT and HF approaches give rather similar evolution of the magnetosubband structure, the corresponding behavior of the total spin polarization $P$ and the effective $g$ factor, $g^{\text{eff}}$, is also similar, see figures 1(c)–(f). (We define the effective $g$ factor according to $g^{\text{eff}} = \langle (E^{\uparrow}_{n,k} - E^{\downarrow}_{n,k})/g\mu_{\text{B}}B \rangle$ where the averaging is performed over all the $k$ vectors and the occupied subbands $n$.) The DFT approach gives a slightly higher value of $P$ at the lower fields because of the enhanced spin polarization near the edges as discussed above. Both approaches give quantitatively similar dependences of $g^{\text{eff}}$ as a function of magnetic field. Because $g^{\text{eff}}$ is directly related to the subband spin splitting, the dependence of $g^{\text{eff}} = g^{\text{eff}}(B)$ closely follows that of $P = P(B)$, showing a well-known oscillatory character with a periodicity of $1/B$ related to the subband depopulation [25]. A maximum value of $g^{\text{eff}} \approx 15$ is reached close to magnetic fields corresponding to depopulation of the even subbands, i.e. when the subband splitting in the wire center is maximal. A similar behavior of the $g$ factor is also manifest in its dependence on $V_0$, see figure 4. Increasing $V_0$ corresponds to the raising of the bottom of the potential which leads to the depopulation the subbands. This, in turn, leads to the oscillatory dependence of $g^{\text{eff}}$ which shows a maximum each time the even subband depopulates. Note that this behavior of $g^{\text{eff}} = g^{\text{eff}}(V_0)$ as well as the absolute value of the $g^{\text{eff}}$ are consistent with the experimental results of Pallecchi *et al* [26] who extracted the $g$ factor of the quantum wire from the magnetocapacitance measurements.

## 4. Conclusion

We demonstrate that the spin DFT and HF approaches provide qualitatively (and, in most cases, quantitatively) the same description of a split-gate quantum wire in the IQH regime. This includes the electron density, spin polarization and the effective $g$ factor. The two approaches give the same magnetic field values for successive subband depopulations and qualitatively similar evolution of the magnetosubbands. Quantitatively, however, the HF and the DFT subbands are different (even though the corresponding total electron densities are practically the same). In contrast to the HF approach, the DFT calculations predict much larger spatial spin separation near the wire edge for the low fields (when the compressible strips for spinless electrons are not formed yet).

## References

[1] Giuliani G F and Vignale G 2005 *Quantum Theory of the Electron Liquid* (Cambridge: Cambridge University Press)
[2] Kinaret J M and Lee P A 1990 *Phys. Rev.* B **42** 11768
[3] Dempsey J, Gelfand B Y and Halperin B I 1993 *Phys. Rev. Lett.* **70** 3639
[4] Tokura Y and Tarucha S 1994 *Phys. Rev.* B **50** 10981
[5] Manolescu A and Gerhardts R R 1995 *Phys. Rev.* B **51** 1703
[6] Heinonen O, Lubin M I and Johnson M D 1995 *Phys. Rev. Lett.* **75** 4110
Ferconi M, Geller M R and Vignale G 1995 *Phys. Rev.* B **52** 16357
[7] Stoof T H and Bauer G E W 1995 *Phys. Rev.* B **52** 12143
[8] Balev O G and Vasilopoulos P 1997 *Phys. Rev.* B **56** 6748
[9] Brataas A, Gudmundsson V, Mal'shukov A G and Chao K A 1998 *J. Phys.: Condens. Matter* **10** 4267
[10] Schmerek D and Hansen W 1999 *Phys. Rev.* B **60** 4485
[11] Zhang Z and Vasilopoulos P 2002 *Phys. Rev.* B **66** 205322
[12] Balev O G, Silva S and Studart N 2005 *Phys. Rev.* B **72** 085345
[13] Struck A, Mohammadi S, Kettemann S and Kramer B 2005 *Phys. Rev.* B **72** 245317
[14] Ihnatsenka S and Zozoulenko I V 2006 *Phys. Rev.* B **73** 075331
[15] Ihnatsenka S and Zozoulenko I V 2006 *Phys. Rev.* B **73** 155314
[16] Ihnatsenka S and Zozoulenko I V 2006 *Phys. Rev.* B **74** 075320
See also for a review: Zozoulenko I V and Ihnatsenka S 2008 *J. Phys.: Condens. Matter* **20** 164217
[17] Römer R A and Sohrmann Ch 2008 *Phys. Status Solidi* b **245** 336
[18] For a review see: Reimann S M and Manninen M 2002 *Rev. Mod. Phys.* **74** 1283
[19] Davies J 1998 *The Physics of Low-Dimensional Semiconductors* (Cambridge: Cambridge University Press)
[20] Tanatar B and Ceperley D M 1989 *Phys. Rev.* B **39** 5005
[21] Chklovskii D B, Shklovskii B I and Glazman L I 1992 *Phys. Rev.* B **46** 4026
Chklovskii D B, Matveev K A and Shklovskii B I 1993 *Phys. Rev.* B **47** 12605
[22] Suzuki T and Ando T 1993 *J. Phys. Soc. Japan* **62** 2986
[23] Muller G, Weiss D, von Klitzing K, Ploog K, Nickel H, Schlapp W and Losch R 1992 *Phys. Rev.* B **46** 4336
[24] Ciorga M, Pioro-Ladriere M, Zawadzki P, Hawrylak P and Sachrajda S A 2002 *Appl. Phys. Lett.* **80** 2177
[25] Ando T, Fowler A B and Stern F 1982 *Rev. Mod. Phys.* **54** 437
[26] Pallecchi I, Heyn Ch, Lohse J, Kramer B and Hansen W 2002 *Phys. Rev.* B **65** 125303